Aerospace Science and Technology ••• (••••) •••–•••

Contents lists available at ScienceDirect

Aerospace Science and Technology

www.elsevier.com/locate/aescte

An adaptive predictor–corrector reentry guidance based on self-definition way-points

En-mi Yong*, Wei-qi Qian, Kai-feng He

CAI, China Aerodynamics Research & Development Center, Mianyang, Sichuan 621000, China

ARTICLE INFO

Article history:
Received 14 March 2013
Received in revised form 6 August 2014
Accepted 13 August 2014
Available online xxxx

Keywords:
Reentry
Guidance
Predictor–corrector
BELBIC
Way-points

ABSTRACT

An adaptive predictor–corrector reentry guidance algorithm with self-defined way-points is proposed. In the guidance process, the reentry trajectory is divided into the predictor–corrector phase and the trajectory onboard generation and tracking phase which is near to the endpoint position of reentry and utilized to improve the accuracy and adaptivity of the guidance. In the first phase, the predictor–corrector algorithm is applied to solve the guidance problem between the self-defined way-points. Moreover the position parameters of reentry trajectory are translated into the parameters related to the reentry plane by orthogonal transformation in the spherical coordinate to improve robustness of guidance algorithm. In addition, the predictor–corrector algorithm is implemented using a brain emotional learning based intelligence controller (BELBIC). In the second phase, the trajectory from the current point to the endpoint is generated onboard and the linear–quadratic regulator (LQR) theory is employed for trajectory tracking. The effectivity of the proposed guidance is validated by simulations in conditions of the nominal case, the environment dispersed case and the endpoint maneuvering case. The advantages of this guidance in coping with disturbances, reducing time of numerical trajectory prediction and being suitable for maneuver endpoint are analyzed with the simulation results.

1. Introduction

Various hypersonic and reentry vehicle technologies are being pursued to enable a prompt global reach ability, such as the Falcon plan vehicle of U.S. Air Force, e.g., the Common Aero Vehicle. The reentry guidance plays an important role in steering the vehicle safely through the dispersed reentry flight environment, while meeting the mission requirements [7]. A high degree of autonomy and adaptability is desirable for future reentry vehicles.

Much of the reentry guidance techniques in development today are influenced by the Space Shuttle reentry guidance. This guidance and other similar acceleration guidances, like drag acceleration planning and tracking guidance, are almost based on the assumption that the vehicle will follow a great circle arc connecting the initial entry point to the target point. So the accuracy of this kind of guidance is reduced at high crossrange [4,9,10,14,19]. The Evolved Acceleration Guidance Logic for Entry (EAGLE) is originally presented by Saraf et al. [15]. It is a direct extension of the Shuttle's longitudinal acceleration guidance to include the lateral dimension. Leavitt improves the EAGLE for its application in suborbital entry scenario [8]. The reference heading angle is also tracked with bank angle as the control variable. However, manual tuning of the trajectory tracking law is needed in EAGLE. It is expected that the need for manual tuning could eventually be eliminated.

Other researchers break away from the traditional drag guidance approach. Dukeman has developed a linear state-feedback longitudinal tracking law [3]. The energy-varying gains are tuned offline using an LQR. Strength of the tracking law is the near trajectory independence of its gain tuning. Zimmerman et al. have developed an onboard trajectory planner [27]. Trajectory design is implemented in two parts. In the earlier part, a constant thermal flux is followed. In the second part, the planner designs a linear bank angle profile with bank reversals to meet the final range, heading, and altitude requirements. Shen and Lu also plan and track complete three-degree-of-freedom entry trajectories [16,17]. The planning occurs onboard before entry. During trajectory design, the entry phase is broken into three sub-phases, the most significant of which is the quasi-equilibrium glide (QEG) phase. Then the authors have developed a trajectory planner for suborbital entry which does not use the QEG assumption [18]. During entry phase, the planned longitude dynamics are followed by tracking law which is similar to Dukeman's guidance. The bank reversals are commanded using the logic similar to the Shuttle's, though the crossrange is used as a reversal criterion instead of heading angle.

* Corresponding author. Tel.: +86 816 2364034.
E-mail address: Emyong@cardc.cn (E.-m. Yong).

http://dx.doi.org/10.1016/j.ast.2014.08.004
1270-9638/

Due to the enhancement of the capability of the computer, the numerical predictor–corrector guidance is developed in the past few decades. Youssef designs a predictor–corrector guidance to handle widely dispersed entry conditions [26]. The control variables are perturbations of the bank angle, the angle-of-attack and the time for roll reversal. The bank angle and the angle-of-attack profiles are the nominal profiles plus the perturbations. The altitude, heading and range errors at terminal area energy management interface are used to correct the initial guess of the control variables. Several perturbed state cases for initial entry conditions and different initial guesses are used to test the performance of the guidance for the X-33 operations. However, the real-time application of the algorithm needs further demonstration. A predictor–corrector guidance algorithm for atmospheric reentry is presented by Joshi et al. [7]. The control variables are parameterized with variation over nominal angle-of-attack (AOA) profile and a bank angle at a predefined velocity for constructing linear variation of the bank angle with respect to relative velocity. Otherwise the guidance methodology includes the path constraint control law as a part of the predictor algorithm, namely the bank angle is modulated when the drag and drag rate of predict trajectory exceed the boundaries decided by path constraints. Xue also develops a constrained predictor–corrector entry guidance algorithm for vehicles with medium to higher lifting capability [22]. The algorithm enforces the path constraints by transforming them into the energy-dependent upper and lower bounds in the velocity-altitude space with the help of quasi-equilibrium glide condition (QEGC) for the magnitude of the bank angle. In addition, the numerical predictor–corrector is used as the core algorithm in newly developed entry guidance for the lifting interplanetary re-entry vehicle and the capsule return from the Moon [1,2,20].

In this paper, an adaptive predictor–corrector reentry guidance based on self-definition way-points is proposed for the medium to high lift-to-drag ratio reentry vehicles. The strategy of the guidance is purposed to improve its performance in crossrange control, adaptivity to disturbed circumstances and dealing with maneuverable target.

2. Outline of the presented guidance strategy

The presented reentry guidance is divided into two phases from the initial point to the endpoint of reentry, as described in Fig. 1. In the first phase (PI), the predictor–corrector guidance between self-defined way-points is implemented. In the second phase (PII), which is near the endpoint, an onboard trajectory generation and tracking guidance is adopted to enhance the adaptability of the guidance. Furthermore, the key points of the guidance strategy are as following:

A. In the predictor–corrector phase, the normal sphere coordinate system is translated to a new sphere coordinate system by orthogonal transformation, in which the plane of zero latitude is coincidence to the reentry plane.

B. The way-points are defined in the new sphere coordinate and generated by the optimal trajectory which is obtained by Gauss pseudospectral method. In addition, the way-points are corresponding to the Gauss nodes of the optimal trajectory.

C. The predictor–corrector algorithm, which is implemented between the self-defined way-points, is developed by the Brain Emotional Learning Based Intelligence Controller for its robustness and less computation time.

D. In the second guidance phase, a three dimensional reference trajectory, from the current position to the endpoint, is generated onboard. And the linear–quadratic regulator is employed for trajectory tracking.

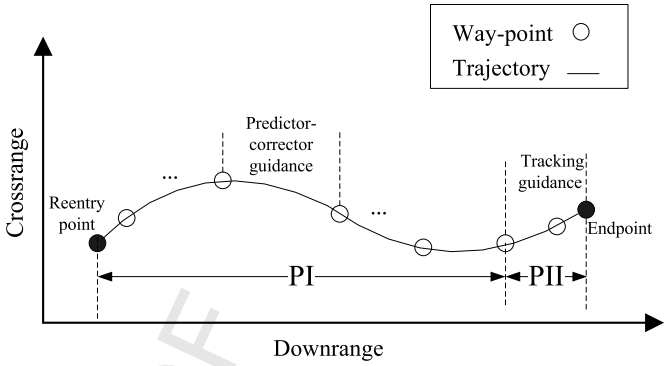

PI: Predictor-corrector Phase
PII: Trajectory generation and tracking phase

Fig. 1. Sketch map of the presented guidance.

3. Coordinate transformation and way-points determination

3.1. Coordinate transformation for guidance

In normal sphere coordinate system, supposing a rotational sphere earth model, we use the radial distance from the center of the earth, longitude and latitude to describe the position of the vehicle relative to the Earth. And we also use the magnitude of velocity, flight path angle and azimuth angel to describe the vehicle velocity relative to the Earth [21]. Here, the motivation is to present a new sphere coordinate to denote the position and velocity of the vehicle relative to reentry plane through orthogonal transformation. The new sphere coordinate is obtained as the following steps.

3.1.1. Orthogonal rotation of sphere coordinate system

Firstly the reference plane can be determined by the two vectors: one is from the center of the Earth to the reentry point, another is from center of the Earth (the same start point) to the endpoint of reentry. Then the sphere coordinate system is rotated to let the zero latitude plane (so called the equatorial plane) be coincidence to the reentry plane. In the new sphere coordinate system, we use $\widehat{\theta}, \widehat{\varphi}, \widehat{r}, \widehat{V}, \widehat{\gamma}, \widehat{\psi}$ to denote the reentry states. According to the definition of reentry plane, the new longitude $\widehat{\theta}$ and the new latitude $\widehat{\varphi}$ can directly indicate the downrange and crossrange of the reentry vehicle respectively. And it is obviously that $\widehat{r} = r, \widehat{V} = V, \widehat{\gamma} = \gamma$. In addition, to establish the dimensionless equations of motion for guidance the r is normalized by the average radius of the Earth $R_0 = 6378$ km and denoted as z. And the Earth relative velocity V is normalized by $V_c = \sqrt{g_0 R_0}$, where $g_0 = 9.81$ m/s^2 and denoted as u. So in dimensionless formulation, we have

$$\widehat{z} = z \qquad \widehat{u} = u \qquad \widehat{\gamma} = \gamma \tag{1}$$

3.1.2. Coordinate transformation

In order to establish the relationship between the normal sphere coordinate system and the transformed one, three rectangular coordinate systems, diagrammed in Fig. 2, are introduced here. Two of them are the Earth frame O–$X_E Y_E Z_E$ and rotated Earth frame O–$\widehat{X}_E \widehat{Y}_E \widehat{Z}_E$. The plane $X_E O Y_E$ is the equatorial plane and the plane $\widehat{X}_E O \widehat{Y}_E$ is the reference reentry plane. So we have the relationship

$$\begin{bmatrix} X_E \\ Y_E \\ Z_E \end{bmatrix} = \begin{bmatrix} r\cos\varphi\cos\theta \\ r\cos\varphi\sin\theta \\ r\sin\varphi \end{bmatrix}, \qquad \begin{bmatrix} \widehat{X}_E \\ \widehat{Y}_E \\ \widehat{Z}_E \end{bmatrix} = \begin{bmatrix} \widehat{r}\cos\widehat{\varphi}\cos\widehat{\theta} \\ \widehat{r}\cos\widehat{\varphi}\sin\widehat{\theta} \\ \widehat{r}\sin\widehat{\varphi} \end{bmatrix} \tag{2}$$

Please cite this article in press as: E.-m. Yong et al., An adaptive predictor–corrector reentry guidance based on self-definition way-points, Aerosp. Sci. Technol. (2014), http://dx.doi.org/10.1016/j.ast.2014.08.004

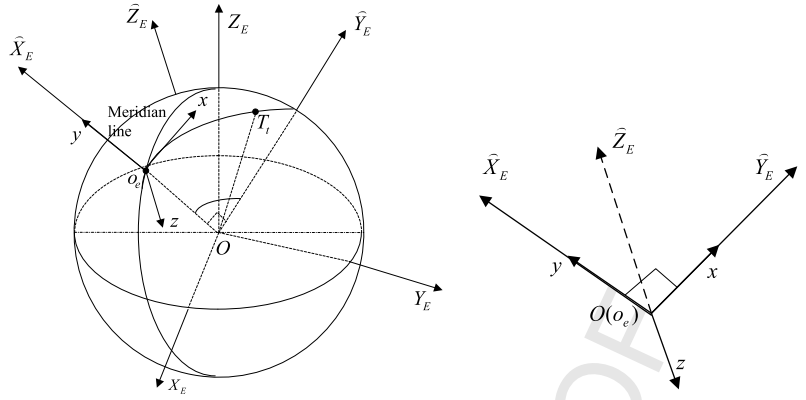

Fig. 2. Three defined frames and relationship of frame o_e–xyz and frame O–$\widehat{X}_E\widehat{Y}_E\widehat{Z}_E$.

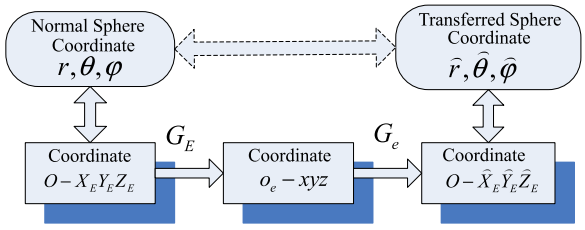

Fig. 3. Transition relationship between coordinate systems.

Next a reentry coordinate system o_e–xyz is introduced and defined as: 1) the origin of the coordinate is the reentry point; 2) the $o_e x$-axis is in the local horizon plane of the point o_e and points to the endpoint; 3) the $o_e y$-axis is perpendicular to the local horizon plane and points to upward direction; 4) the $o_e z$-axis completes a right-handed rectangular coordinate system.

The transition matrix, from the Earth frame O–$X_E Y_E Z_E$ to the reentry frame o_e–xyz is [5]

$$\boldsymbol{G}_E = \boldsymbol{M}_2\left[-\left(A_0 + 90^\circ\right)\right]\boldsymbol{M}_1[\varphi_0]\boldsymbol{M}_3\left[\left(\varphi_0 - 90^\circ\right)\right] \tag{3}$$

Where A_0 is the deviation angle of reentry plane from the north direction and $M_i[\lambda]$ denotes the coordinate transition element Euler matrix which is relative to a coordinate rotating along the i-th axis with the λ angle. The azimuth angle A_0 can be calculated as

$$A_0 = \begin{cases} \arcsin\left(\dfrac{\cos\varphi_T \sin\theta_{0T}}{\sin\widehat{\beta}}\right), & \sin\varphi_T - \cos\widehat{\beta}\sin\varphi_0 \geq 0 \\ \operatorname{sign}\{\arcsin\left(\dfrac{\cos\varphi_T \sin\theta_{0T}}{\sin\widehat{\beta}}\right)\}\pi - \arcsin\left(\dfrac{\cos\varphi_T \sin\theta_{0T}}{\sin\widehat{\beta}}\right), & \sin\varphi_T - \cos\widehat{\beta}\sin\varphi_0 < 0 \end{cases} \tag{4}$$

Where

$$\begin{cases} \theta_{0T} = \theta_T - \theta_0 \\ \widehat{\beta} = \arccos(\sin\varphi_0 \sin\varphi_T + \cos\varphi_0 \cos\varphi_T \cos\theta_{0T}) \end{cases}$$

In Eqs. (3)–(4), the subscripts 0 and T denote the reentry point states and the endpoint states respectively.

It is convenient to translate the base o_E to the base O to establish the transition matrix from frame o_e–xyz to frame O–$\widehat{X}_E\widehat{Y}_E\widehat{Z}_E$ (also see Fig. 2), that is

$$\boldsymbol{G}_{\widehat{E}} = \boldsymbol{M}_3\left[-90^\circ\right]\boldsymbol{M}_1\left[-180^\circ\right] \tag{5}$$

Hence we have the transformation matrix equation from the coordinate O–$X_E Y_E Z_E$ to the coordinate O–$\widehat{X}_E\widehat{Y}_E\widehat{Z}_E$. Furthermore, the relationship between the normal sphere coordinate system and the transformed one can be derived, as described in Fig. 3. So we have

$$\begin{bmatrix} \widehat{r}\cos\widehat{\varphi}\cos\widehat{\theta} \\ \widehat{r}\cos\widehat{\varphi}\sin\widehat{\theta} \\ \widehat{r}\sin\widehat{\varphi} \end{bmatrix} = \boldsymbol{G}_{\widehat{E}} \cdot \boldsymbol{G}_E \begin{bmatrix} r\cos\varphi\cos\theta \\ r\cos\varphi\sin\theta \\ r\sin\varphi \end{bmatrix} = \boldsymbol{G}\begin{bmatrix} r\cos\varphi\cos\theta \\ r\cos\varphi\sin\theta \\ r\sin\varphi \end{bmatrix} \tag{6}$$

Where

$$\boldsymbol{G} = \begin{bmatrix} \cos\varphi_0\cos\theta_0 & \cos\varphi_0\sin\theta_0 & \sin\varphi_0 \\ -\sin A_0\sin\theta_0 - \cos A_0\sin\varphi_0\cos\theta_0 & \sin A_0\cos\theta_0 - \cos A_0\sin\varphi_0\sin\theta_0 & \cos A_0\cos\varphi_0 \\ \cos A_0\sin\theta_0 - \sin A_0\sin\varphi_0\cos\theta_0 & -\cos A_0\cos\theta_0 - \sin A_0\sin\varphi_0\sin\theta_0 & \sin A_0\cos\varphi_0 \end{bmatrix}$$

In addition, the velocity azimuth angle $\widehat{\psi}$ is defined as the angle between velocity vector and the reentry plane, that is

$$\widehat{\psi} = \psi - A_0 \tag{7}$$

So with Eq. (1), Eq. (6) and Eq. (7) the dimensionless kinematical equation of motion in transformed sphere coordinate can be achieved, see Eq. (A.5). The details are described in Appendix A.

3.2. Way-points determination in the transformed sphere coordinate system

Before in the above work we design an optimal trajectory via a Gauss pseudospectral method (GPM) in normal sphere coordinate system. The method is proposed by Yong et al. [25]. Then a trajectory in transferred coordinate system can be obtained through submitting the control variable $\alpha(\tau), \sigma(\tau)$ into equations of motion (A.5) simultaneously let $\widehat{\theta}_0 = 0^\circ, \widehat{\varphi}_0 = 0^\circ$. And other initial parameters can be determined by Eqs. (1) and (7).

Then the trajectory states for guidance application corresponding to the Gauss node can be saved as way-points, including longitude, latitude, dimensionless velocity, dimensionless radial distance and bank angle, signed as $(\widehat{\theta}^i_{Ref}, \widehat{\varphi}^i_{Ref}, \widehat{u}^i_{Ref}, \widehat{z}^i_{Ref}, \sigma^i_{Ref})$. In Fig. 4, simulation results provide the comparison of trajectory and way-points before and after coordinate transformation. It indicates that the position states are transitioned to reentry plane relative ones. And it's helpful to adaptivity of the guidance algorithm.

4. Predictor–corrector algorithm between way-points

4.1. Description of guidance problem between way-points

The guidance algorithm in phase I is implemented not between initial point and endpoint, like the ordinary predictor–corrector guidance, but between adjacent way-points.

The dimensionless energy of the i-th way-point is defined as

$$\widehat{e}^i_{Ref} = \widehat{u}^{i\,2}_{Ref}/2 - 1/\widehat{z}^i_{Ref} \tag{8}$$

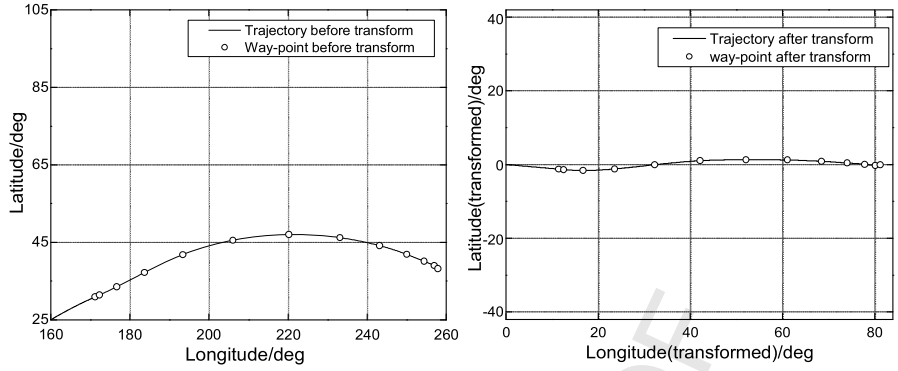

Fig. 4. Comparison of trajectory and way-points before and after transformation.

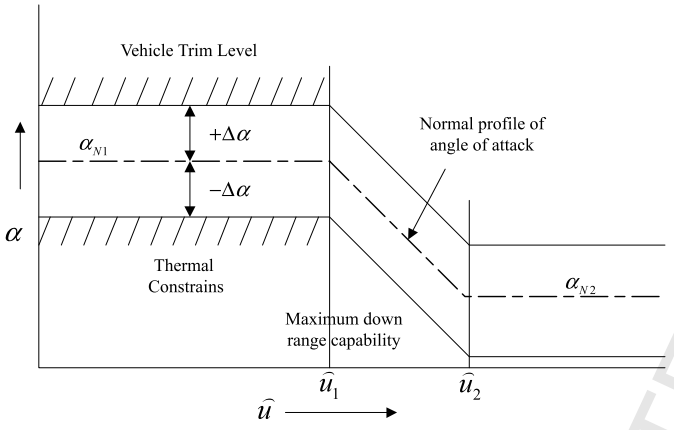

Fig. 5. AOA profile.

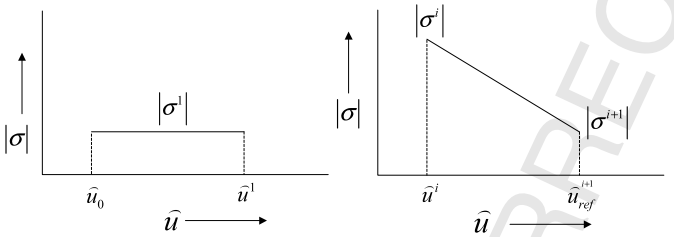

a. $|\sigma|$ in initial descent b. $|\sigma|$ after the 2nd way-point

Fig. 6. Bank angle magnitude profile between way-points.

The guidance problem between way-points can be described as: using the states of the i-th way-point $\boldsymbol{x}^i = (\widehat{z}^i, \widehat{\theta}^i, \widehat{\varphi}^i, \widehat{u}^i, \widehat{\gamma}^i, \widehat{\psi}^i)$ as the initial condition to calculate the bank angle $\sigma(\widehat{u})$ and the angle-of-attack $\alpha(\widehat{u})$ so that the trajectory can satisfy the position constraints of the next way-point

$$\left|\widehat{\theta}^{i+1} - \widehat{\theta}_{Ref}^{i+1}\right| \le \delta\widehat{\theta}, \quad \left|\widehat{\varphi}^{i+1} - \widehat{\varphi}_{Ref}^{i+1}\right| \le \delta\widehat{\varphi} \tag{9}$$

when $\widehat{e} = \widehat{e}_{ref}^{i+1}$ and the path constraints of heat rate, dynamic pressure and aerodynamic load factor.

4.2. Modeling of control parameters

To obtain the trajectory control variables, $\alpha(\widehat{u})$ and $\sigma(\widehat{u})$ should be parameterized.

4.2.1. Parameterized model of angle-of-attack

The normal profile of AOA is designed as the linear function of dimensionless velocity. Here, $\alpha_{N1}, \alpha_{N2}, \widehat{u}_1$ and $\widehat{u}_2$ are predefined values [23]. With the control parameter $\Delta\alpha$, the instantaneous value of α can be determined by normal profile and $\Delta\alpha$, showed in Fig. 5. It is used in trajectory propagation of the predictor in the whole reentry duration.

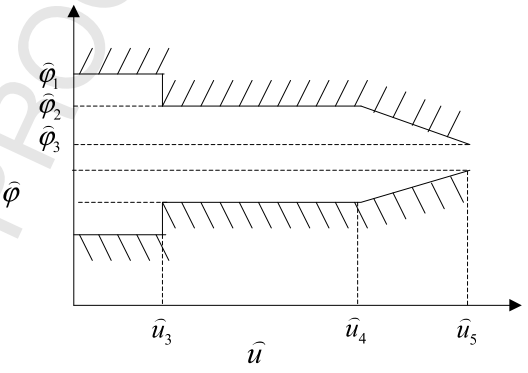

Fig. 7. Crossrange boundary for bank reverse logic.

4.2.2. Parameterized model of bank angle

The model of the magnitude of bank angle $|\sigma|$ is given in Eq. (10) and the corresponding Fig. 6, where e_{ref}^i and $\widehat{u}_{Ref}^{i+1}$ are the i-th predefined dimensionless energy and velocity of the way-points, and $|\sigma^i|$ is the magnitude of bank angle of the i-th way-point to be solved. In the first part, the initial descent phase of reentry, we use a constant magnitude of bank angle $|\sigma^1|$ to modulate trajectories [16]. Thus a linear model of bank angle magnitude between way-points is adopted in the rest of predictor–corrector phase, which is a quasi-equilibrium glide phase.

$$\left|\sigma(\widehat{u})\right| = \begin{cases} |\sigma^1| & \widehat{e} \le e_{ref}^1 \\ |\sigma^{i+1}| + \frac{\widehat{u} - \widehat{u}_{Ref}^{i+1}}{\widehat{u}^i - \widehat{u}_{Ref}^{i+1}}(|\sigma^i| - |\sigma^{i+1}|) & e^i \le \widehat{e} \le e_{ref}^{i+1} \end{cases} \quad i = 1, 2, \cdots N_{pt} \tag{10}$$

Bank reversal logic is employed to determine the sign of σ for trajectory prediction. In transformed sphere coordinate, the new latitude $\widehat{\varphi}$ stands for the crossrange and is directly utilized to construct the boundary function of bank reversal, as described in Eq. (11) and Fig. 7. The numerical simulation indicates that the bank reversal logic is not very sensitive to the boundary. Hence these parameters $\widehat{\varphi}_1, \widehat{\varphi}_2, \widehat{\varphi}_3, \widehat{u}_3, \widehat{u}_4, \widehat{u}_5$ are predetermined in this guidance.

$$|\widehat{\varphi}_{\max}| = \begin{cases} \widehat{\varphi}_1 & \widehat{u} \ge \widehat{u}_3 \\ \widehat{\varphi}_2 & \widehat{u}_4 \le \widehat{u} < \widehat{u}_3 \\ \widehat{\varphi}_2 + (\widehat{u} - \widehat{u}_4)(\widehat{\varphi}_3 - \widehat{\varphi}_2)/(\widehat{u}_5 - \widehat{u}_4) & \widehat{u} < \widehat{u}_4 \end{cases} \tag{11}$$

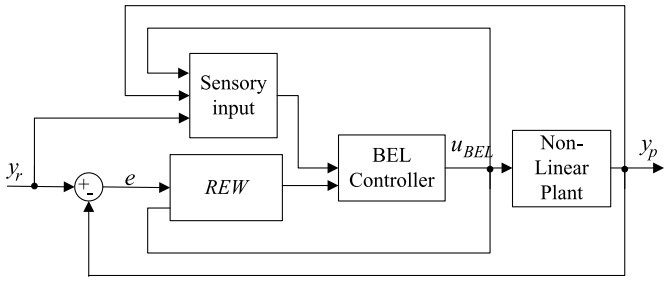

Fig. 8. Architecture of BEL controller [11].

With summarizing the above models we know that the control parameters for the predictor–corrector reentry guidance are $\Delta\alpha, |\sigma^1|$ and $|\sigma^{i+1}|$ $(i = 1, 2, \cdots N_{pt})$, where N_{pt} is the number of way-points.

4.3. Predictor–corrector algorithm based on BELBIC

The general numerical predictor–corrector algorithm based on Newton iteration method, which is very sensitive to the initial value, is difficult to implement in real time on the computer of reentry vehicles at present. In this research, an intelligence controller, BELBIC, is used to develop a high performance predictor–corrector algorithm. Due to the learning ability of BELBIC, it is very powerful in stabilizing and fast in converging to an appropriate control signal. In addition the iteration is not needed in BELBIC. The applications show very good adaptability and robustness of the intelligence controller. It is also proven to be very effective controller with less computation time.

4.3.1. Introduction of BELBIC

Recently, a computational model of emotional learning in mammalians brain has been proposed by Moren and Balkenius [12,13]. Using proposed model a control algorithm has been introduced, which is called BELBIC, and has been successfully employed in design making and control for simple linear systems as well as nonlinear systems. The applications show very good adaptability and robustness of the intelligence controller. The detail of BELBIC computational model can be found in [11].

4.3.2. The controller for predictor–corrector

4.3.2.1. Architecture of BEL controller Inputs to emotional learning mechanism are a set of sensory input signals as well as a reinforcing signal. These signals generally can be arbitrarily selected by the designer of the control algorithm. It is recommended that the reinforcing signal *REW* is a function of the other signals which can be supposed as a cost function rationale, specifically award and punishment

$$REW = f_1(e, u_{BEL}) \tag{12}$$

Where $e(e = y_r - y_p)$ is the error signal and u_{BEL} is the control output. y_r and y_p are the reference output and the plant output respectively.

Similarly the sensory inputs must be a function of plant outputs, reference outputs and controller outputs are as follows

$$S_i = f_2(y_p, y_r, u_{BEL}) \tag{13}$$

The architecture of BEL controller is shown in Fig. 8. As illustrated in [11], sensory input and reward signal are inputs of intelligence controller and can be an arbitrary function of y_r, y_p, u_{BEL} and e. It is all up to the designer to find a proper function for control.

Table 1
Inputs of the intelligence controllers.

Controller	Design variable	*REW*	Sensory inputs S_i
BEL1	$\Delta\alpha$	$k_{\alpha1}\delta\widehat{\theta}^{i+1} + k_{\alpha2}\delta\widehat{u}^{i+1}$	$f_1(\widehat{\theta}_{Ref}^{i+1}, \widehat{\theta}_p^{i+1}, \Delta\alpha)$
BEL2	$\Delta\sigma^{i+1}$	$k_{\sigma1}\delta\widehat{\varphi}^{i+1} + k_{\sigma2}\delta\widehat{u}^{i+1}$	$f_2(\widehat{\varphi}_{Ref}^{i+1}, \widehat{\varphi}_p^{i+1}, \Delta\sigma^{i+1})$

4.3.2.2. BELBIC for predictor–corrector guidance The BELBIC is required to amend the control variables according to system outputs to approach reference outputs whereas the initial value of control variable is not given in the controller. So it is recommended that using increment of the control variable as the design variable of BIEBIC. Thus we decompose the bank angle into two parts: the reference value, which comes from the predetermined optimal trajectory in the way-points, and the incremental value, that is to say $|\sigma^{i+1}| = |\sigma_{ref}^{i+1}| + \Delta\sigma^{i+1}$, where $|\sigma_{ref}^{i+1}|$ is the predetermined $|\sigma|$ at every way-point. And the sign of the bank angle is still decided by bank reversal logic. Then we design two intelligence controllers, denoted as BEL1 and BEL2, to calculate the guidance variables $\Delta\alpha$ and $\Delta\sigma^{i+1}$. The *REW* and sensory inputs of the two controllers are listed in Table 1. The errors of the downrange and the crossrange are reflected in *REW*. And the sensory inputs are functions of the target position, the prediction position and the controller outputs as follows:

$$\begin{aligned} &f_1 : S_{\alpha1} = k_{\alpha_3}\widehat{\theta}_{Ref}^{i+1}; \quad S_{\alpha2} = k_{\alpha_4}\widehat{\theta}_p^{i+1}; \quad S_{\alpha2} = k_{\alpha_5}\Delta\alpha \\ &f_2 : S_{\sigma1} = k_{\sigma_3}\widehat{\varphi}_{Ref}^{i+1}; \quad S_{\sigma2} = k_{\sigma_4}\widehat{\varphi}_p^{i+1}; \quad S_{\sigma3} = k_{\sigma_5}\Delta\sigma^{i+1} \end{aligned} \tag{14}$$

In one guidance circle, the inputs of intelligence controllers (BEL1, BEL2) can be obtained by trajectory predicting, which implements numerical integration once from the current state to the next way-point state. The outputs of the controllers consequently become the control variables of the predictor–corrector guidance.

4.4. Path constraints implementation in predictor–corrector algorithm

The feasible region of reentry trajectories is specified by path constraints of heating rate, aerodynamic load, dynamic pressure and QEG. To ensure the guided trajectory to satisfy these constraints, these requirements are converted to the constraint of bank angle and implemented in trajectory predictor. This work is completed by Yong et al. [24] and will not list here for the length limitation.

5. Trajectory generation and tracking in PII

The former works are all for the first phase guidance. To enhance the adaptability of the guidance algorithm, we propose an onboard trajectory generation and tracking algorithm in the second phase (PII) which is close to the endpoint. The triggering condition of the phase II is

$$S_{togo} \le S_{Gen} \tag{15}$$

where S_{togo} is the rang-to-go of the current time and S_{Gen} is the total range of the second guidance phase. In this research, S_{Gen} is set as about one-tenth of the total reentry range.

The onboard reference trajectory generation is executed several seconds before phase II by a Gauss pseudospectral method which is presented by the author in Ref. [16].

Dukman's tracking law using LQR is employed for trajectory tracking in the phase II. The dimensionless equations of motion are linearized at the reference profiles to get the linear time-varying

Table 2
Reentry interface of nominal reentry condition.

Velocity (m/s)	Altitude (km)	Flight path angle (deg)	Longitude (deg)	Latitude (deg)	Velocity azimuth angle (deg)
7200	100	−2	160	5/15/25/50	55/55/52/62

Table 3
Parameters of BELBIC.

Controller	Design variable	*REW*	S_i	Learning rate
BEL1	$\Delta\alpha$	$k_{\alpha 1}=10, k_{\alpha 2}=8$	$k_{\alpha_3}=4, k_{\alpha_4}=6, k_{\alpha 5}=1$	$\alpha_a=4\times10^{-4}, \alpha_o=5\times10^{-5}$
BEL2	$\Delta\sigma^{i+1}$	$k_{\sigma 1}=10, k_{\sigma 2}=10$	$k_{\sigma_3}=3, k_{\sigma 4}=5, k_{\sigma_3}=1$	$\alpha_a=3\times10^{-4}, \alpha_o=5\times10^{-5}$

Table 4
Results in nominal condition ($Ts=1$ s).

	Location error with respect to endpoint (km)			Time parameters (s)		
	Downrange	Crossrange	Altitude	*TP*	*TA*	*TG*
case1	1.23	2.740	0.13	0.15	36.77	4.98
case2	2.824	1.737	0.72	0.15	45.9	5.51
case3	0.898	−0.341	0.35	0.21	53.1	4.66
case4	3.593	−0.529	0.53	0.36	50.2	4.68

dynamics. The control variable for trajectory tracking is $\delta\mathbf{U}$ and we have

$$\mathbf{U}=\mathbf{U}_{ref}+\delta\mathbf{U}=\begin{bmatrix}\sigma_{ref}+\delta\sigma\\ \alpha_{ref}+\delta\alpha\end{bmatrix} \tag{16}$$

Where σ_{ref} and α_{ref} are bank angle and AOA of reference trajectory.

The general description of the LQR and corresponding tracking law will not listed here and can be found in [3].

6. Performance of the proposed guidance algorithm

To evaluate the performance of the proposed reentry guidance algorithm, detailed numerical simulations are carried out with the following four conditions: 1) nominal condition in different reentry interface; 2) perturbation condition considering the dispersion reentry interface; 3) perturbation condition considering the disturbance of aerodynamic coefficients, air density, mass of vehicle and combination of them; 4) maneuvering endpoint position condition.

6.1. Assumptions and design parameters for simulation

The assumptions and main design parameters used for verification of the algorithm are as follows:

A. The trajectory prediction adopts the dimensionless 3DOF equations of motion (A.5). Then the 4-th Runge–Kutta integral method is used for numerical integration. The simulation is executed in the software environment of MATLAB.

B. According to the principle of BELBIC, only one trajectory prediction is implemented in one guidance circle which is taken as 1 s or 2 s.

C. The allowable terminal error in range and altitude is $\leq$10 km and $\leq$2 km respectively. The range error for way-points arriving is $\leq$10 km.

D. The predefined parameters of AOA profile are: $\alpha_{N1}=20$ deg, $\alpha_{N2}=10$ deg, $V_1=4762$ m/s (corresponding to $\widehat{u}_1$), $V_2=3067$ m/s (corresponding to $\widehat{u}_2$). And the limitation of the regulation magnitude of α in guidance is $\Delta\alpha\leq5$ deg.

E. The parameters of crossrange error corridors shown in Eq. (11) are $\widehat{\varphi}_1=1.5$ deg, $\widehat{\varphi}_2=0.8$ deg, $\widehat{\varphi}_3=0.2$ deg, $V_3=7000$ m/s (corresponding to $\widehat{u}_3$), $V_4=3000$ m/s (corresponding to $\widehat{u}_4$), $V_5=750$ m/s (corresponding to $\widehat{u}_5$).

F. The boundary of the bank angle is -80 deg $\leq\sigma\leq80$ deg.

G. Path constraints: heat rate limit $=1000$ kW/m^2, g-load limit $=2$, dynamic pressure limit $=120$ kPa.

H. The aerodynamic model is constructed by that of U.S. Air force concept vehicle of Common Aero Vehicle [?].

I. The CPU time of the guidance cycle, the maximum predictor–corrector time in all guidance cycles, the total prediction time, and the onboard trajectory generation time is denoted as *Ts*, *TP*, *TA* and *TG* respectively in the following simulation results.

6.2. Performance in nominal condition

Four different cases of reentry conditions are considered, as given in Table 2, in nominal condition simulation. And the same endpoint position is used in the four cases. The endpoint longitude, latitude and height is 258°, 38° and 20 km respectively.

The control parameters of BELBIC, including reinforcing signal *REW*, sensory input S_i and learning rate, are all listed in Table 3. From the simulation of guidance performance we know that the learning rate is the most influential parameter of them. It also indicates that too large learning rate will lead to shaking in design variables $\Delta\alpha$ and $\Delta\sigma^{i+1}$ whereas too small one will result in reduction of guidance accuracy. The parameters in Table 2 obtained from several simulation tests are suitable for the proposed guidance problem and also applied in the rest numerical simulations.

The summaries of simulation results for the four cases are given in Table 4 and Fig. 9. These results show that the guidance algorithm achieves the terminal conditions with specified accuracy, while simultaneously satisfying the path constraints. And the first two figures of Fig. 9 show that the concept of the proposed guidance is effective. The time properties of guidance algorithm are also given in Table 4. In the first guidance phase, the maximum predict time between way-points is less than half of 1 s while the guidance circle is set as 1 s. It indicates that the prediction time is less than the guidance circle in the numerical simulation. In the second guidance phase, the trajectory onboard generation time is within several seconds. This guidance algorithm is implemented in MATLAB software. So it is potential to reduce computational time by using some highly effective language like C++.

6.3. Performance under dispersion reentry interface

To assess the performance of the guidance algorithm under conditions of dispersed reentry interface, simulations are carried out with assumed dispersions on the reentry initial states, as given

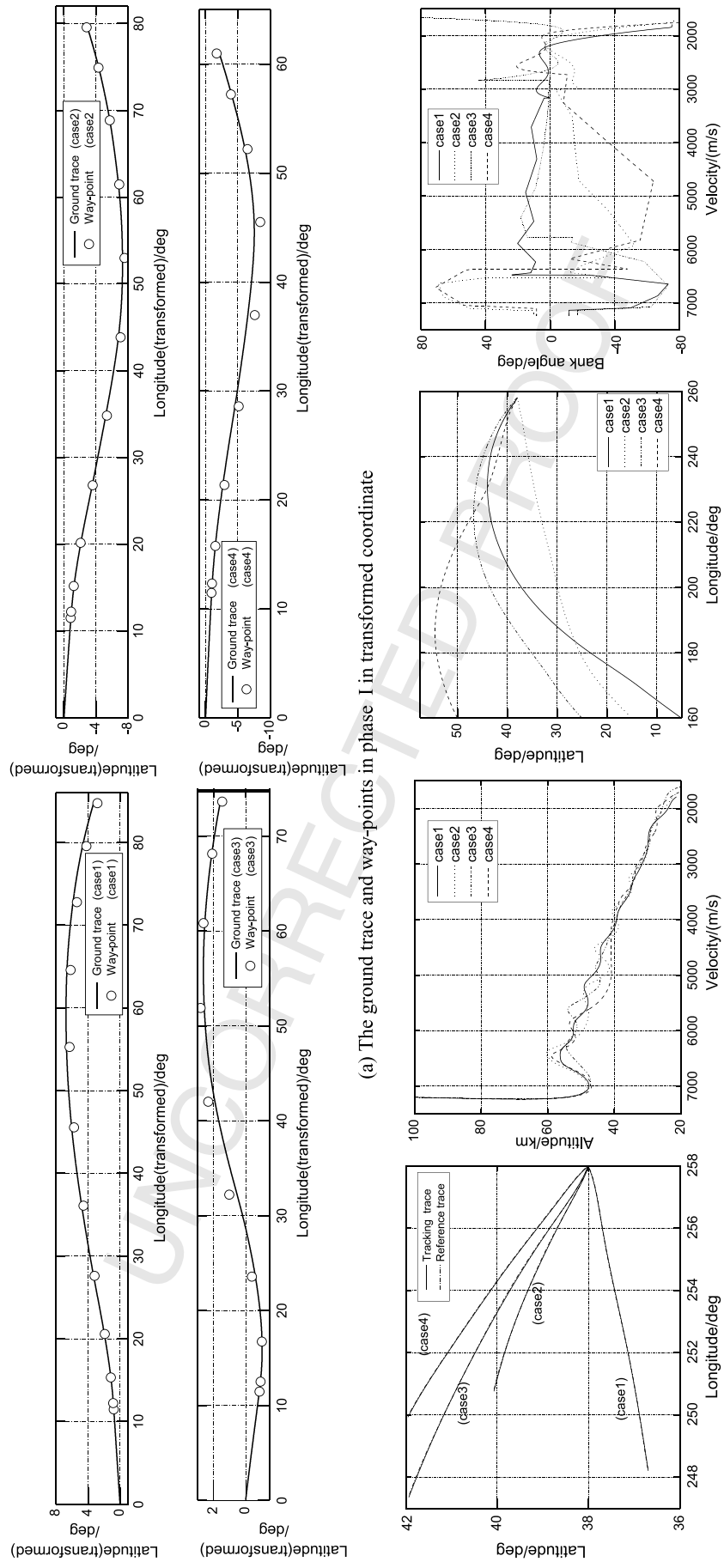

Fig. 9. Simulation results of the four cases in nominal condition.

in Table 5. The corresponding states and steering profiles are given in Fig. 10. These results show that the bank angle and AOA are modulated to meet the terminal conditions. The time parameters are also listed in Table 5 and are similar with the simulation results in the normal condition in quality. It is seen that the influence of interface disturbance to prediction time is not obvious.

6.4. Performance under disturbed flight environment

The robustness of the proposed guidance algorithm is also validated by the simulation under off-normal environment conditions considering the disturbance of aerodynamic coefficients, air density, mass of vehicle and combination of them. Table 6 gives the details of the off-normal conditions and the summaries of the simulation results. The corresponding states and steering profiles are given in Fig. 11. It is found that the presented algorithm achieves the same level of accuracy in the off-nominal environment compared to the simulations in the nominal conditions. Furthermore, it seems that the uncertainty of aerodynamic coefficient exercise more influence on the guidance accuracy than the disturbance of the air density and the vehicle mass.

6.5. Performance for maneuvering endpoint condition

The proposed guidance is designed to deal with the situation that the endpoint of reentry phase deviates from the original position in the range of 100 km before the second guidance phase. When the deviation range is larger, this guidance problem can be settled by increasing S_{Gen} in Eq. (15). And the onboard trajectory generation algorithm will also be suitable when S_{Gen} becomes longer. This aspect of robustness of this guidance is benefit from the trajectory onboard generation strategy in the second guidance phase. Three cases of maneuvering endpoint conditions and simulation results in guidance accuracy and time properties are given in Table 7. The corresponding trajectory and steering angle profiles are given in Fig. 12. These results show that a and σ are suitably modulated to meet the terminal conditions with the specify accuracy in the maneuvering endpoint position condition. Furthermore, the trajectory generation time is also about several seconds, which is the same magnitude of time as the above simulation cases.

7. Conclusion

This paper has presented an adaptive predictor–corrector reentry guidance algorithm for atmospheric reentry vehicles with middle to high lift-to-drag ratio. The performance of simulations in nominal reentry condition validate the efficiency of the guidance strategy which executes a predictor–corrector algorithm between self-defined way-points and a trajectory onboard generation and tracking law in two guidance phases in the sequence. The robustness of the algorithm is evaluated by simulations considering dispersions on reentry interface, environment and maneuvering endpoint position condition respectively.

Different kinds of perturbation, including varied reentry interface, environment disturbance and maneuvering endpoint distance, are considered. It is seen that the disturbance on aerodynamic lift and drag exercise the most influence on guidance accuracy. Also, it is seen that the trajectory onboard generation and tracking law do much benefits on improving guidance accuracy on the condition of maneuvering endpoint position. Furthermore, the implementation of the predictor–corrector algorithm between way-point, not from the reentry interface to the endpoint like the general predictor–corrector algorithm, increases the efficiency of the guidance algorithm. It results in much less time of the predictor–corrector than that of the guidance circle.

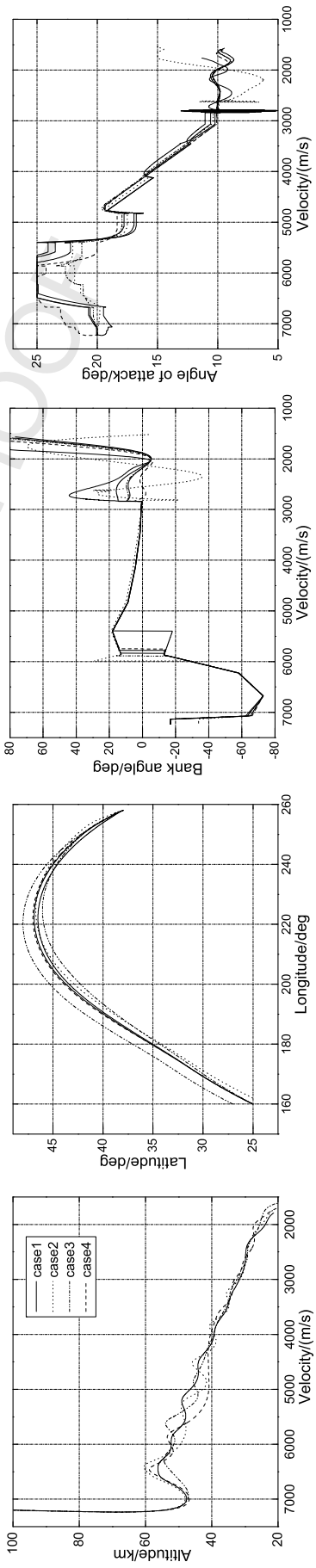

Fig. 10. Simulation results of varying reentry interface conditions.

Table 5
Results in disturbance of reentry point condition ($Ts = 1$ s).

Dispersion case	Location error with respect to endpoint (km)			Time parameters(s)		
	Downrange	Crossrange	Altitude	*TP*	*TA*	*TG*
Altitude + 2 km	1.61	−1.57	0.113	0.17	67.0	4.37
Velocity − 30 m/s	1.85	−2.05	0.011	0.24	82.9	4.74
$\theta + 2$ deg	0.611	0.329	0.548	0.18	52.26	6.06
$\varphi + 2$ deg	4.13	−5.56	1.482	0.17	49.21	5.61
$\gamma - 0.2$ deg	2.11	−1.96	0.213	0.21	77.92	4.18
$\psi + 2$ deg	1.52	−1.66	−0.144	0.18	64.6	5.89

Table 6
Results in disturbance of flight environment.

Dispersion case	Location error with respect to endpoint (km)			Time parameters (s)		
	Downrange	Crossrange	Altitude	*TP*	*TA*	*TG*
$C_D - 10\%$	0.497	−8.103	−0.697	−0.2	92.48	3.72
$C_D + 10\%$	2.30	−6.57	−0.081	0.16	81.50	4.77
$C_L - 10\%$	2.29	−2.57	−0.081	0.36	89.59	5.19
$C_L + 10\%$	0.659	−7.168	−0.566	0.43	92.1	5.08
$m + 5\%$	2.74	−2.08	−0.161	0.22	62.13	4.99
$m - 5\%$	2.19	−2.68	−0.377	0.34	67.88	4.33
$\rho + 25\%$	2.40	−3.37	1.477	0.25	82.16	4.0
$\rho - 25\%$	2.09	1.79	−1.471	0.40	93.45	4.16
$C_L, C_D - 10\%$ $\rho - 25\%$, $m - 5\%$	1.53	4.90	−0.127	0.34	92.77	4.56
$C_L, C_D + 10\%$ $\rho + 25\%$, $m + 5\%$	1.91	−1.98	−0.015	0.24	82.57	4.22

Table 7
Results of maneuvering endpoint condition.

Endpoint case	Deviation of endpoint (km)	Location error with respect to endpoint (km)		Time parameters (s)		
		Downrange	Crossrange	*Ts*	*TA*	*TG*
T1	69.0	2.24	−1.81	1	67.0	4.37
T2	68.8	1.28	−1.46	1	82.9	6.75
T3	92.9	2.21	−3.66	2	52.26	5.42

The next step is to demonstrate how efficiently this algorithm can be coded and how effective it is when it is used in the 6-DOF flight simulation including Monte Carlo simulation.

Conflict of interest statement

None declared.

Acknowledgements

The authors wish to acknowledge Dr. Zhendong Hu for his valuable suggestions and discussions during the development of the algorithm. The first author would like to thank Mr. Chen for improving the expression of English.

Appendix A. Derivation for equations of motion in transferred frame

According to Eq. (6), we can obtain

$$\begin{aligned}
\cos\widehat{\varphi}\cos\widehat{\theta} &= G_{11}\cos\varphi\cos\theta + G_{12}\cos\varphi\sin\theta + G_{13}\sin\varphi \\
\cos\widehat{\varphi}\sin\widehat{\theta} &= G_{21}\cos\varphi\cos\theta + G_{22}\cos\varphi\sin\theta + G_{23}\sin\varphi \\
\sin\widehat{\varphi} &= G_{31}\cos\varphi\cos\theta + G_{32}\cos\varphi\sin\theta + G_{33}\sin\varphi
\end{aligned} \tag{A.1}$$

And let two sides of Eq. (6) multiply the inverse matrix of **G**, we can get

$$\begin{bmatrix} G_{11} & G_{12} & G_{13} \\ G_{21} & G_{22} & G_{23} \\ G_{31} & G_{32} & G_{33} \end{bmatrix}^{-1} \begin{bmatrix} \widehat{r}\cos\widehat{\varphi}\cos\widehat{\theta} \\ \widehat{r}\cos\widehat{\varphi}\sin\widehat{\theta} \\ \widehat{r}\sin\widehat{\varphi} \end{bmatrix} = \begin{bmatrix} r\cos\varphi\cos\theta \\ r\cos\varphi\sin\theta \\ r\sin\varphi \end{bmatrix} \tag{A.2}$$

Denoting that

$$\begin{bmatrix} G_{11} & G_{12} & G_{13} \\ G_{21} & G_{22} & G_{23} \\ G_{31} & G_{32} & G_{33} \end{bmatrix}^{-1} = \begin{bmatrix} G'_{11} & G'_{12} & G'_{13} \\ G'_{21} & G'_{22} & G'_{23} \\ G'_{11} & G'_{11} & G'_{11} \end{bmatrix} \tag{A.3}$$

we have

$$\begin{aligned}
\sin\varphi &= G'_{31}\cos\widehat{\varphi}\cos\widehat{\theta} + G'_{32}\cos\widehat{\varphi}\sin\widehat{\theta} + G'_{33}\sin\widehat{\varphi} \\
&\triangleq B_3(\widehat{\theta},\widehat{\varphi}) \\
\cos\varphi\cos\theta &= G'_{11}\cos\widehat{\varphi}\cos\widehat{\theta} + G'_{12}\cos\widehat{\varphi}\sin\widehat{\theta} + G'_{13}\sin\widehat{\varphi} \\
&\triangleq B_1(\widehat{\theta},\widehat{\varphi}) \\
\cos\varphi\sin\theta &= G'_{21}\cos\widehat{\varphi}\cos\widehat{\theta} + G'_{22}\cos\widehat{\varphi}\sin\widehat{\theta} + G'_{23}\sin\widehat{\varphi} \\
&\triangleq B_2(\widehat{\theta},\widehat{\varphi})
\end{aligned} \tag{A.4}$$

Where B_1, B_2, B_3 are the temporary variables in derivation. So the trigonometric function of the longitude θ and latitude φ of the reentry vehicle can be expressed with B_1, B_2, B_3. The unpowered reentry dynamics in transferred spherical coordinate can be derived with Eqs. (1), (7), (A.4) and the dimensionless equations of motion in original sphere coordinate listed in [17], given as

$$\begin{aligned}
\frac{d\widehat{z}}{d\tau} &= \widehat{u}\sin\widehat{\gamma} \\
\frac{d\widehat{\varphi}}{d\tau} &= \frac{\widehat{u}\cos\widehat{\gamma}}{\widehat{z}\cos\widehat{\varphi}\sqrt{B_1^2 + B_2^2}} \\
&\quad\cdot\left[-G_{31}\left(B_3B_1\cos\left(A_0+\widehat{\psi}\right) + B_2\sin\left(A_0+\widehat{\psi}\right)\right)\right. \\
&\quad + G_{32}\left(B_1\sin\left(A_0+\widehat{\psi}\right) - B_3B_2\cos\left(A_0+\widehat{\psi}\right)\right) \\
&\quad \left. + G_{33}\left(B_1^2 + B_2^2\right)\cos\left(A_0+\widehat{\psi}\right)\right]
\end{aligned}$$

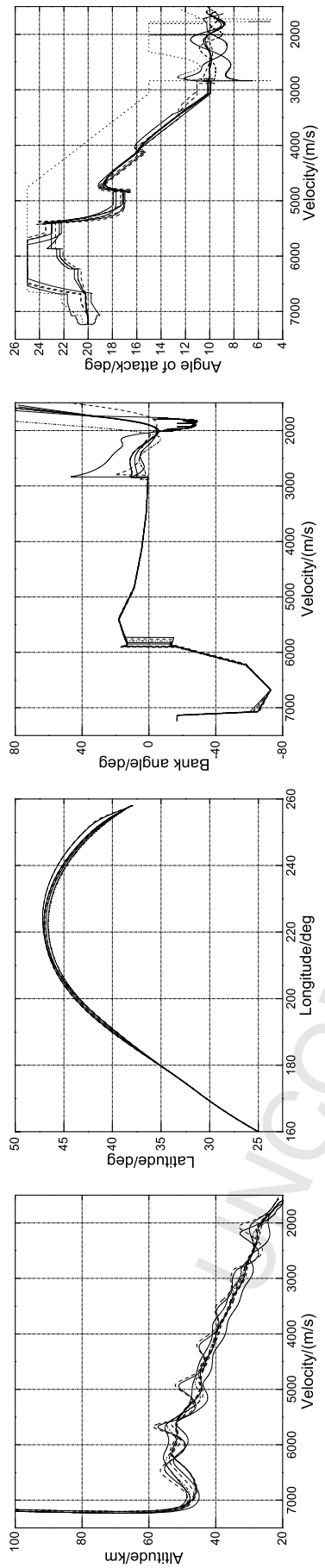

Fig. 11. Simulation results of dispersed flight environment.

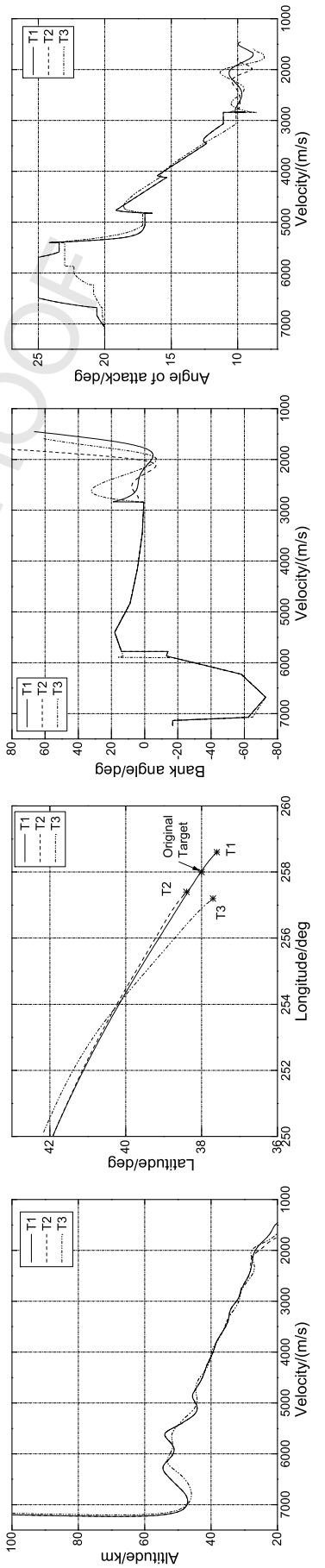

Fig. 12. Simulation results of the maneuvering endpoint position condition.

$$
\begin{aligned}
\frac{d\widehat{\theta}}{d\tau} &= \frac{\widehat{u}\cos\widehat{\gamma}}{\widehat{z}\cos\widehat{\varphi}\cos\widehat{\theta}\sqrt{B_1^2+B_2^2}} \\
&\quad\cdot\Big\{\big(B_3B_1\cos\big(A_0+\widehat{\psi}\big)+B_2\sin\big(A_0+\widehat{\psi}\big)\big) \\
&\quad\cdot\left(-G_{31}\frac{\sin\widehat{\varphi}\sin\widehat{\theta}}{\cos\widehat{\varphi}}-G_{21}\right) \\
&\quad+\big(B_1\sin\big(A_0+\widehat{\psi}\big)-B_3B_2\cos\big(A_0+\widehat{\psi}\big)\big) \\
&\quad\cdot\left(G_{32}\frac{\sin\widehat{\varphi}\sin\widehat{\theta}}{\cos\widehat{\varphi}}+G_{22}\right)+\big(B_1^2+B_2^2\big)\cos\big(A_0+\widehat{\psi}\big) \\
&\quad\cdot\left(\frac{\sin\widehat{\varphi}\sin\widehat{\theta}}{\cos\widehat{\varphi}}G_{33}+G_{23}\right)\Big\} \\
\frac{d\widehat{\gamma}}{d\tau} &= \frac{1}{\widehat{u}}\Big[\bar{L}\cos\sigma+\frac{\cos\widehat{\gamma}}{\widehat{z}}\left(\widehat{u}^2-\frac{1}{\widehat{z}}\right) \\
&\quad+2\Omega\widehat{u}\sqrt{B_1^2+B_2^2}\sin\big(A_0+\widehat{\psi}\big) \\
&\quad+\Omega^2\widehat{z}\Big(\cos\widehat{\gamma}\big(B_1^2+B_2^2\big) \\
&\quad+\sin\widehat{\gamma}\cos\big(A_0+\widehat{\psi}\big)B_3\sqrt{B_1^2+B_2^2}\Big)\Big] \\
\frac{d\widehat{u}}{d\tau} &= -\bar{D}-\frac{\sin\widehat{\gamma}}{\widehat{z}^2}+\Omega^2\widehat{z}\Big(\sin\widehat{\gamma}\big(B_1^2+B_2^2\big) \\
&\quad-B_3\sqrt{B_1^2+B_2^2}\cos\widehat{\gamma}\cos\big(A_0+\widehat{\psi}\big)\Big) \\
\frac{d\widehat{\psi}}{d\tau} &= \frac{1}{\widehat{u}}\Big[\frac{\bar{L}\sin\sigma}{\cos\widehat{\gamma}}+\frac{\widehat{u}^2}{\widehat{z}}\frac{B_3\cos\widehat{\gamma}\sin(A_0+\widehat{\psi})}{\sqrt{B_1^2+B_2^2}} \\
&\quad-2\Omega\widehat{u}\Big(\tan\widehat{\gamma}\cos\big(A_0+\widehat{\psi}\big)\sqrt{B_1^2+B_2^2}-B_3\Big) \\
&\quad+\frac{\Omega^2\widehat{z}}{\cos\widehat{\gamma}}\frac{B_3B_1}{\sqrt{B_1^2+B_2^2}}\sin\big(A_0+\widehat{\psi}\big)\Big]
\end{aligned}
\tag{A.5}
$$

Uncited references

[6]

References

[1] M.I. Afzal, H. Roeser, M. Graesslin, An explicit guidance method for a lifting interplanetary re-entry vehicle, in: AIAA Guidance, Navigation, and Control Conference, Chicago, Illinois, 2009, AIAA-2009-6108.
[2] J.L. Davis, A.D. Cianciolo, R.W. Powell, Guidance and control algorithms for the Mars entry, descent and landing systems analysis, in: AIAA/AAS Astrodynamics Specialist Conference, Ontario, Canada, 2010, AIAA-2010-7972.
[3] G.A. Dukeman, Profile-following entry guidance using linear quadratic regulator theory, in: AIAA Guidance, Navigation, and Control Conference and Exhibit, Monterey, California, 2002, AIAA-2002-4457.
[4] J.C. Harpold, C.A. Graves, Shuttle entry guidance, J. Astronaut. Sci. 27 (3) (1979) 239–268.
[5] P.R. Jia, K.J. Chen, L. He, Longrange Rocket Trajectory Theory, Press of National University of Defense Technology, Changsha, 1997, pp. 7–16.
[6] T.R. Jorris, Common Aero Vehicle autonomous reentry trajectory optimization satisfying waypoints and no-fly zone constraints, Dissertation, PhD thesis, Air Force Institute of Technology, Air University, 2007.
[7] A. Joshi, K. Sivan, S.S. Amma, Predictor–corrector reentry guidance algorithm with path constraints for atmospheric entry vehicles, J. Guid. Control Dyn. 30 (5) (2007) 1307–1318.
[8] J.A. Leavitt, Advanced entry guidance algorithm with landing footprint computation, Dissertation, PhD thesis, University of California Irvine, 2005.
[9] P. Lu, Entry guidance and trajectory control for reusable launch vehicle, J. Guid. Control Dyn. 20 (1) (1997) 143–149.
[10] P. Lu, J.M. Hanson, Entry guidance for the X-33 vehicle, J. Spacecr. Rockets 35 (3) (1998) 342–349.
[11] A.R. Mehrabian, C. Lucas, Emotional learning based intelligent robust adaptive controller for stable uncertain nonlinear systems, Int. J. Comput. Intell. 2 (4) (2006) 246–251.
[12] J. Moren, Emotion and learning—a computational model of the amygdala, Dissertation, PhD thesis, Lund University, 2002.
[13] J. Moren, C. Balkenius, A computational model of emotional learning in the amygdala, from animals to animals, in: Proceedings of the 6th International Conference on the Simulation of Adaptive Behavior, Cambridge, Mass. 2000.
[14] A.J. Roenneke, A. Markl, Reentry control of a drag vs. energy profile, J. Guid. Control Dyn. 17 (5) (1994) 916–920.
[15] A. Saraf, J.A. Levitt, D.T. Chen, et al., Design and evaluation of an acceleration guidance algorithm for entry, J. Spacecr. Rockets 41 (6) (2004) 986–996.
[16] Z. Shen, P. Lu, Onboard generation of three-dimensional constrained entry trajectories, J. Guid. Control Dyn. 26 (1) (2003) 111–121.
[17] Z. Shen, P. Lu, Dynamic lateral entry guidance logic, J. Guid. Control Dyn. 27 (6) (2004) 949–959.
[18] Z. Shen, P. Lu, Onboard entry trajectory planning expanded to sub-orbital flight, AIAA-2003-5736, 2003.
[19] K.-Y. Tu, M.S. Munir, K.D. Mease, et al., Drag-based predictive tracking guidance for Mars precision landing, J. Guid. Control Dyn. 23 (4) (2000) 620–628.
[20] P. Vernis, F. Spreng, G. Gelly, et al., Accurate skip-entry guidance for low to medium L/D spacecrafts return missions requiring high range capabilities, in: AIAA Guidance, Navigation, and Control Conference, Portland, Oregon, 2011, AIAA-2011-6649.
[21] N.X. Vinh, A. Busemann, R.D. Culp, Hypersonic and Planetary Entry Flight Mechanics, University of Michigan Press, Ann Arbor, 1980, pp. 19–28.
[22] S. Xue, P. Lu, Constrained predictor–corrector entry guidance, J. Guid. Control Dyn. 33 (4) (2010) 1273–1281.
[23] E.M. Yong, L. Chen, G.J. Tang, Trajectory optimization of hypersonic gliding reentry vehicle based on the physical programming, Acta Aeronaut. Astronaut. Sin. 29 (5) (2008) 1091–1097.
[24] E.M. Yong, G.J. Tang, L. Chen, Rapid trajectory planning for hypersonic unpowered long-range reentry vehicles with multi-constraints, J. Astronaut. 29 (1) (2008) 46–52.
[25] E.M. Yong, W.Q. Qian, K.F. He, Trajectory optimization of lifting-type reentry vehicle via Gauss pseudospectral method, in: 62nd International Astronautical Congress, Cape Town, 2011.
[26] H. Youssef, R.S. Chowdhry, L. Howard, et al., Predictor–corrector entry guidance for reusable launch vehicles, in: AIAA Guidance, Navigation, and Control Conference and Exhibit, Montreal, Canada, 2001, AIAA-2001-4043.
[27] C. Zimmerman, G.A. Dukeman, J.M. Hanson, Automated method to compute orbital reentry trajectories with heating constraints, J. Guid. Control Dyn. 26 (4) (2003) 523–529.